Temperature dependence of the ferromagnetic response in $Cr_xSb_{2-x}Te_3$ topological insulator thin films investigated using terahertz spectroscopy and magneto-transport

Varun Kamboj[a,], Angadjit Singh[a], Lukas Jakob[a,c], Liam B. Duffy[b], Satyaprasad P. Senanayak[a], Harvey E. Beere[a], Adrian Ionescu[a], Crispin H.W. Barnes[a], Thorsten Hesjedal[b], David A. Ritchie[a]*

[a]*Cavendish Laboratory, University of Cambridge, J. J. Thomson Avenue, Cambridge CB3 0HE, United Kingdom*
[b]*Clarendon Laboratory, Department of Physics, University of Oxford, Oxford OX1 3PU, United Kingdom*
[c]*Institute of Physical and Theoretical Chemistry, University of Tuebingen, 8, 72076 Tuebingen, Germany*

(Invited Paper)

ABSTRACT

Introducing a magnetic dopant in a topological insulator can give rise to ferromagnetic ordering which can break time-reversal symmetry, realizing dissipationless electronic states in the absence of an external magnetic field. Assessment and control of the magnetic state can translate into novel future applications in quantum computing. We provide a detailed systematic study of the magnetic state in highly doped $Cr_xSb_{2-x}Te_3$ thin films using terahertz time-domain spectroscopy and electrical transport. The temperature dependent behavior of the THz conductance of $Cr_xSb_{2-x}Te_3$ thin films with x = 0.15 exhibits a clear insulator-metal transition at T_c ~ 40 K, indicating the ferromagnetic order in the $Cr_xSb_{2-x}Te_3$ occurs via the carrier-mediated RKKY mechanism. Moreover, the magneto-transport measurements showed anomalous Hall behaviour below 40 K, demonstrating the consistency between the electrical and optical measurements. Using THz optical means, the direct correlation obtained between the carrier density and ferromagnetism in the magnetically doped topological insulators films, strongly suggests a carrier-mediated Ruderman-Kittel-Kasuya-Yoshida (RKKY) coupling scenario. Our non-contact means of investigating ferromagnetism using THz, and consistency in optical and electrical measurements paves the way to realise exotic quantum states for spintronic and low energy magneto-electronic device applications.

Keywords: topological insulators, THz spectroscopy, Cr:Sb_2Te_3, ferromagnetism, anomalous Hall effect, RKKY interaction

1. INTRODUCTION

One of the most important discovers in the condensed matter physics during the 1980s established that electrons confined in two dimensions and subject to a strong magnetic field display an original 'topological' order, due to the so-called quantum Hall effect.[1] Over the past few years it has been found that such a topological order also occurs in certain three-dimensional (3D) insulating materials. The term "topological insulator" (TI) was first introduced in 2007 to generalize the two-dimensional quantum spin Hall state to three dimensions.[2,3] The non-trivial topology of the band structure[4] arising from time reversal symmetry (TRS) and spin-momentum locking[4,5] leads to the formation of gapless conducting surface and edge states, resistant to scattering by defects and impurities. This has prompted a substantial research effort to look for exotic quantum phenomena exploiting the topological nature of carriers in these materials, potentially revolutionizing the field of condensed matter. Transition metal doping in TIs is predicted to break TRS which opens a surface gap at the Dirac point[6,7]. This has led to the recent experimental observations of the topological magnetoelectric effect[8], induction of a magnetic monopole[9] and the quantum anomalous Hall effect (QAHE)[10]. Hence a wide range of potential industrial applications have been demonstrated in literature such as magnetic sensing[11], information storage[11], phase change memories[12] and various spin injectors for spintronic devices[13]. In the quantized version of the anomalous Hall effect (AHE), the topologically protected state has a dissipationless current flowing along the edge of a 2D surface of a magnetically doped TI in the absence of a magnetic field. In this context, Cr-doped Sb_2Te_3 has been the object of consideration since

*E-mail: vk302@cam.ac.uk , Phone: +44 1223 768142

the discovery that it becomes ferromagnetic when Cr replaces Sb.[14] The AHE has been previously investigated in transition metal doped dilute magnetic semiconductors (DMS) and complex oxide ferromagnets[15], and various theories have also been prescribed[15] to determine the general origin of the AHE. In TIs, on the other hand, it is now well established that the origin of the AHE relies on a scattering-independent, intrinsic mechanism which can be described in terms of the Berry phase effect in crystal momentum space[10, 15-17]. The evolution of the AHE with temperature and magnetic field can be linked to the magnetization, *M*, of the sample through the following relationship[15]: $\rho_{xy} = R_o B + R_s M$, where ρ_{xy} is the total Hall resistivity, B is the applied magnetic field, $R_o = 1/nec$ (e being the electron charge and n the carrier concentration) is the ordinary Hall coefficient arising from the Lorentz force experienced by electrons/holes, and R_s is the anomalous Hall coefficient. Rearranging the terms, equation expresses the summation of the Hall currents, that is, the total Hall conductivity $\sigma_{xy}{}^{T} = \frac{\rho_{xy}}{\rho_{xx}{}^{2} + \rho_{xy}{}^{2}} \approx \frac{\rho_{xy}}{\rho_{xx}{}^{2}} = \frac{RoB + R_S M}{\rho_{xx}{}^{2}}$ with $\sigma_{xy}{}^{T} = \sigma_{xy}{}^{O} + \sigma_{xy}{}^{A}$, where $\sigma_{xy}{}^{O}$ and $\sigma_{xy}{}^{A}$ are the ordinary and anomalous Hall conductivity respectively. These result in: $\sigma_{xy}{}^{A} = \sigma_{xy}{}^{T} - \sigma_{xy}{}^{O} = \frac{R_S M}{\rho_{xx}{}^{2}}$. Therefore, the magnetisation *M* can be accurately determined from $\sigma_{xy}{}^{A}$ the by carefully removing the ordinary Hall component $\sigma_{xy}{}^{O} = \frac{R_O B}{\rho_{xx}{}^{2}}$ from $\sigma_{xy}{}^{T}$, hence enabling the field and temperature dependence in *M* to be extracted directly from magnetotransport data. Within this framework, there is also a strong motivation to understand the mechanism of the magnetic behaviour in TIs. Historically the two most prevalent models in the literature have been: the Van Vleck mechanism[18] which is caused by the large spin susceptibility of the valence electrons in the band-inverted TI materials and the Rudderman-Kittel-Kasuya-Yosida (RKKY)[6] coupling, where the interaction between two localised spins is mediated with the assistance of itinerant carriers. Consequently, the former is independent of the carrier density and is referred as "bulk ferromagnetism", while in the latter case the neighbouring magnetic moments couple via a carrier-mediated mechanism. Controlling the magnetic properties of doped TIs as a function of temperature provides a direct route to investigate the mechanism of the magnetic behaviour in TIs. Recently, $Cr_xSb_{2-x}Te_3$ magnetic topological insulator (MTI) samples, were characterized using x-ray magnetic circular dichroism (XMCD) and carrier mediated coupling was observed.[19] In addition, it was also reported that a good crystalline order is maintained in molecular beam epitaxy (MBE) grown ~60 quintuple layer (QL) thick films of $Cr_xSb_{2-x}Te_3$ (x = 0.15, 0.26, 0.42) using x-ray diffraction (XRD) and atomic force microscopy.[14] In this study, we present a comprehensive comparison of the variation in ferromagnetism in doped $Cr_xSb_{2-x}Te_3$ films (x ranging from 0.15 to as high as 0.76) through terahertz time domain spectroscopy and electrical transport measurements. We present results suggesting the ferromagnetic order in the films is via the carrier-mediated RKKY mechanism.

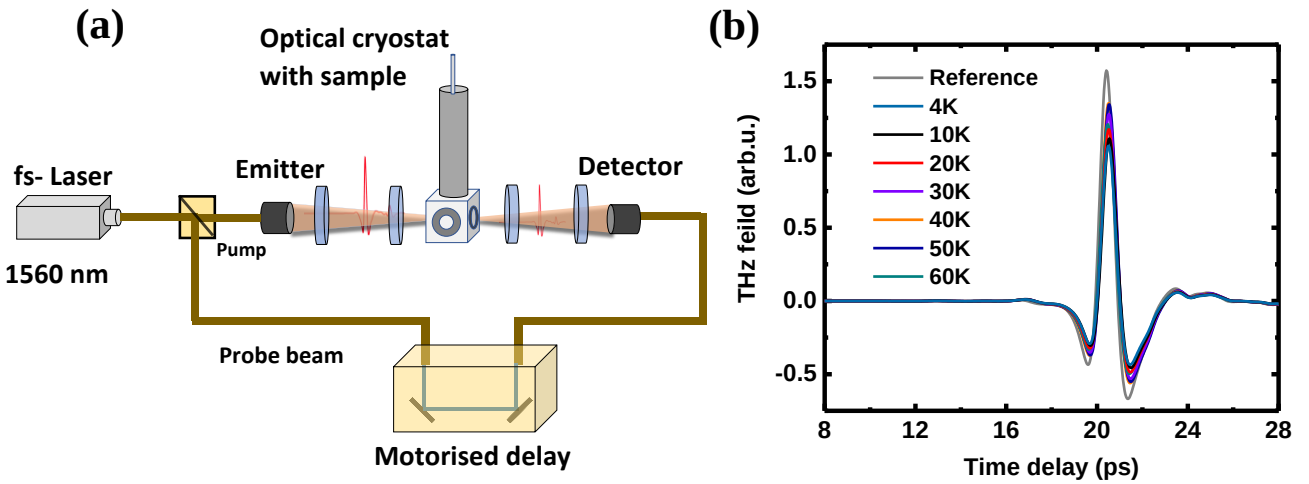

Figure 1. (a) Schematic of a THz-TDS optical setup. A 60-mW pump laser output of 90 fs duration, centered at 1560 nm, was split into two paths for THz generation (pump) and detection (probe). (b) Time domain picosecond (ps) pulse response transmitted through Bi_2Se_3 film of 23 QL (quintuple layer) thickness at different temperatures. The inset shows a magnified pulse response transmitted through the Bi_2Se_3 film. The reference is the transmission through a blank (0001)-oriented sapphire substrate, obtained at 200 K. All the temperature measurements were performed in a cryostat with optical access with a base temperature of 4 K.

2. GROWTH AND TEMERATURE DEPENDENT RESPONSE: $Cr_{0.15}Sb_{1.85}Te$

The Cr-doped Sb_2Te_3 thin films with a characteristic thickness of 20 nm were grown by MBE in an ultra-high vacuum chamber (UHV) with a base pressure lower than 2×10^{-10} Torr using a two-step growth method. High purity Sb (6N) and Te (6N) were co-evaporated from standard effusion cells together with a high temperature cell for Cr (5N) to obtain high quality stoichiometric Cr-doped Sb_2Te_3. In the first phase a 5-nm-thick, undoped Sb_2Te_3 seed layer (see Ref. [15]) was grown. The flux ratio of Te per (Sb + Cr) was maintained at ~10:1. An overpressure of Te flux ensured reduction in vacancies during the growth, commonly observed in this material system[20]. The Cr doping concentration was controlled accurately by adjusting the cell temperature to grow the subsequent 15 nm of Cr-doped Sb_2Te_3. The Cr concentrations were found to follow approximately the measured beam flux monitor fluxes. The typical growth rate for our experiment was ~1 quintuple layer/minute (QL/min). To conclude, a 3-nm-thick amorphous Te capping layer was grown at room temperature prior to taking the sample out of ultra-high vacuum to avoid any contamination and oxidation of the Cr-doped Sb_2Te_3 films.

Broadband terahertz time domain spectroscopy was carried out on $Cr_xSb_{2-x}Te_3$, using a Tera K15-T-Light MENLO system. A schematic of the optical arrangement is illustrated in Figure 1(a). A 60-mW (max power) pump laser with 90 fs pulse duration centred at 1560 nm (repetition rate of 100 MHz) was divided into two optical beam paths: (i) first the beam was focused down to a sub-50 μm spot onto the THz emitter, resulting in a broadband THz emission with a spot size of ~1 mm (at 1THz), and (ii) the second beam went through the delay stage for coherent THz detection. The temperature dependent measurements were carried out using a Janis continuous flow cryostat with optical access capable of reaching a base temperature of 4 K. We performed temperature dependent THz-TDS on the $Cr_{0.15}Sb_{1.85}Te_3$ sample (lowest Cr concentration) to obtain conductance response as a function of temperature, optically in the quasi d.c. limit. The time-resolved THz transmission through the $Cr_{0.15}Sb_{1.85}Te_3$ thin film was measured at various temperatures as shown in Figure 1(b). The transmitted THz field intensity initially increases with reducing temperature down to 40 K, because of a reduced free carrier absorption, implying the freezing out of bulk charge carries. Below 40 K, the transmitted intensity reduces with decreasing temperature, indicating the onset of an interaction distinct from the response of bulk carriers. However, the response is still strongly dependent on the surrounding 'charge carrier sea', resulting in the observed temperature variation. Thus, a drop in the THz transmission is symptomatic of a RKKY mediated transport below 40 K in $Cr_{0.15}Sb_{1.85}Te_3$ film.

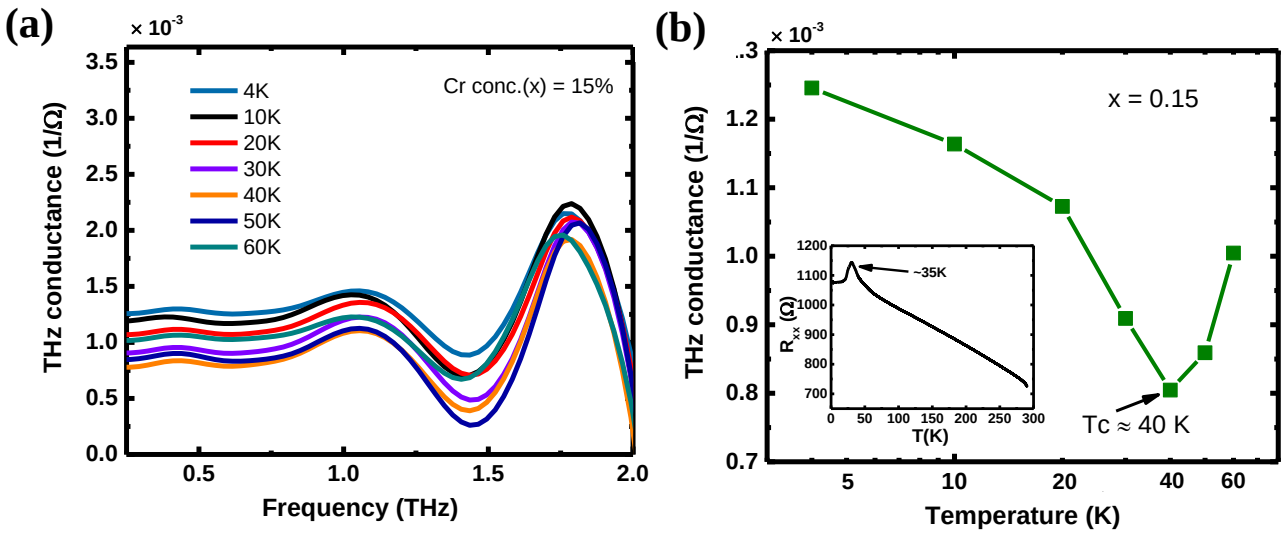

Figure 2. (a) THz conductance spectra of $Cr_{0.15}Sb_{1.85}Te_3$ at different temperatures with a distinct feature at ~1.8 THz referring to the optical phonon mode. (b) THz (quasi-d.c.) conductance at THz as a function of temperature. The inset shows the longitudinal resistance vs. temperature response for the $Cr_{0.15}Sb_{1.85}Te_3$ thin film, obtained from the transport measurements.

To examine the distinct signature of the magnetic state at low temperatures we calculated the optical conductance of the $Cr_{0.15}Sb_{1.85}Te_3$ thin film using Tinkham's theory[21] to obtain the spectral response as presented in Fig. 2 (a). In the ultrathin-film limit, THz conductance spectra were obtained from the normalized transmission (for a detailed description see Ref. 27). The THz conductance spectra in Figure 2(a) shows a typical Drude type response with a characteristic phonon signature at around 1.8 THz, consistent with previous reports of THz measurements on Sb_2Te_3 and other TIs[22,23].

Figure 2(b) shows the THz conductance response of $Cr_{0.15}Sb_{1.85}Te_3$ plotted as a function of temperature. As the temperature is reduced from 60 K down to 40 K, the THz conductance decreases rapidly indicating a freezing of the bulk carriers in the magnetically doped TI film. However, the THz conductance begins to gradually increase with a further reduction in temperature because of an insulator-to-metal transition at ~ 40 K. Such a behaviour can be attributed to the spin disorder scattering that sets in at the paramagnetic to ferromagnetic transition.[24,25] The temperature (~40 K) obtained from our THz measurements is in close agreement with the T_c value obtained the resistance vs. temperature plot (~35 K) from the Hall transport shown in the inset of Figure 2(b). Introducing a magnetic dopant in TI results in breaking of the time reversal symmetry[26] and a bulk insulator type response would be expected from the film (conductance decreasing with decreasing temperature). However below 40 K, the THz conductance shows a metallic response (increasing conductance), indicating an increased carrier-assisted coupling between magnetic ions in the film, therefore suggesting that the magnetism in $Cr_{0.15}Sb_{1.85}Te_3$ could be RKKY mediated.

To investigate the transition observed at ~40 K in the THz response, magneto-transport measurements were carried out on the 20-QL-thick $Cr_{0.15}Sb_{1.85}Te_3$. For this, samples processed in the form of Hall bars devices, to electrically characterize the ferromagnetic ordering response in $Cr_{0.15}Sb_{1.85}Te_3$. A larger piece of wafer was cleaved into smaller chips of dimension 5 mm × 5 mm, in a clean room environment. Standard S1813 photoresist was spin coated onto the sample, followed by an optical lithography process using a mask pattern and an aligner. Micrometre sized Hall bar geometries of dimensions L = 800 µm and W = 200 µm were produced, schematically shown in the inset of Figure 3(a). The mesa was then defined using Ar ion milling in a vacuum chamber with a calibrated rate of ~100 Å/min. 20/80 nm of Ti/Au were then evaporated as Ohmic contacts for the Hall bar in a thermal evaporator, followed by a standard lift-off process with acetone and isopropanol. The chips were then glued to the leadless chip carriers (LCCs) and Au wires were used to bond the contacts onto the pads using a ball bonder.

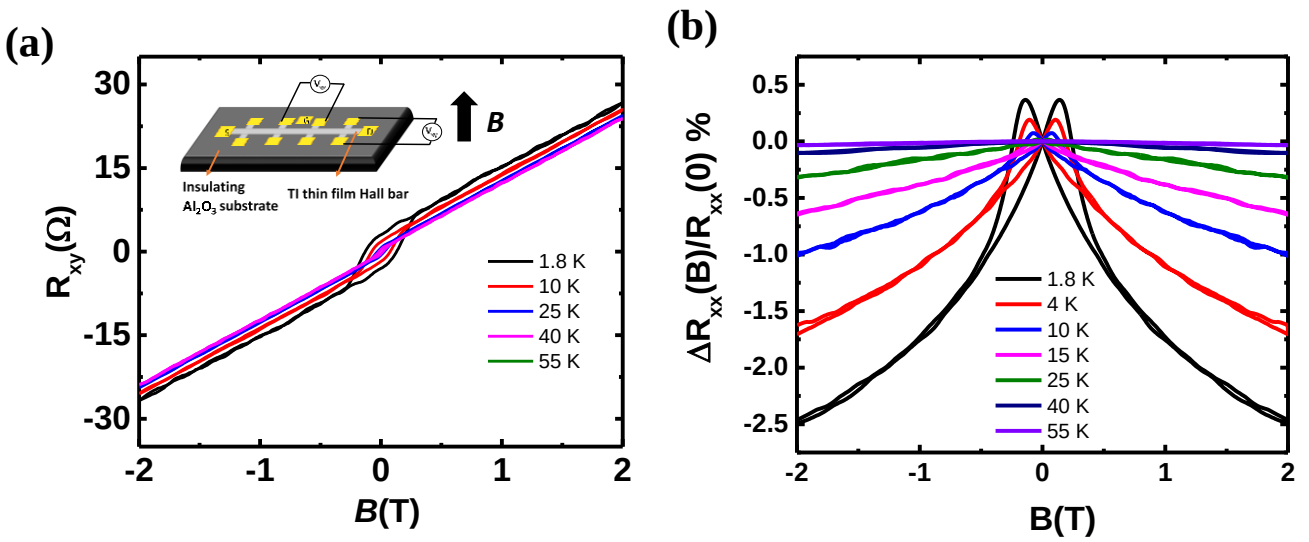

Figure 3. (a) Hall resistance R_{xy} in $Cr_xSb_{2-x}Te_3$ samples with x = 0.15 showing hysteretic behaviour, corresponding to the anomalous Hall effect at different temperatures from 1.8 K to 55 K. The inset shows a schematic of the fabricated Hall bar device. (b) Temperature-dependent negative magnetoresistance ratio for 20-nm-thick $Cr_xSb_{2-x}Te_3$ sample with x = 0.15 due to spin dependent scattering of carriers.

The sample was secured to a probe and dipped into a continuous flow cryostat with a base temperature of 1.8 K equipped with a 9 T superconducting magnet. The Hall, R_{xy}, and longitudinal, R_{xx}, resistances were measured using a standard AC lock-in four-terminal method with the current applied in-plane and the magnetic field perpendicular to the film. All measurements were carried out with an excitation current of 1 μA at a frequency of 77 Hz. The magneto-transport measurements down to 1.8 K resulted in Hall traces showing that $Cr_xSb_{2-x}Te_3$ film has hole-type carriers with $x = 0.15$. Figures 3(a) shows the evolution of the Hall resistance, R_{xy}, as a function of temperature and magnetic field, *B*. Clear, long-range ferromagnetic ordering indicating the easy axis of orientation pointing out-of-plane is observed in the transport measurements. We also performed the Hall transport, R_{xy}, with changing the directions of the magnetic field, *B*, with respect to the sample (θ changes from out-of-plane $\theta = 90°$ to in-plane $\theta = 0°$) and found that the slope gradually changes from positive to negative until we see a parabolic dependence at $\theta = 0°$. This parabolic behaviour at $\theta = 0°$ indicates a strong out-of-plane spontaneous magnetization at zero field, confirming that the magnetic moments of the sample prefer to be in the perpendicular direction. This feature may be favourable for spintronic applications, where perpendicular magnetic anisotropy is more common than in plane magnetism[27,28]. The carrier density at obtained from the Hall slope was ~ 5.8×10^{13} cm^{-2}, while the mobility was ~207.2 cm^2/Vs.

Figures 3(b) illustrate the *B*-dependent magnetoresistance (MR) ratio $\frac{\delta R}{R_0} = \frac{R(B)-R_{xx}(0)}{R_{xx}(0)}$ measured from 55 K to 1.8 K. The butterfly shaped hysteresis exemplifies the negative MR which is caused by spin dependent scattering of carriers[29] as local magnetic ordering comes into play at T_c. The distance between the two peaks for all temperatures corresponds to the coercive field H_c. T_c can be estimated as the temperature when H_c becomes approximately zero. At this point, the long-range ordering disappears, and a positive *MR* is observed corresponding the weak anti-localization (WAL) commonly observed in pristine TI samples[30,31]. An undoped 20-nm-thick Sb_2Te_3 sample was measured for comparison with the doped film. The longitudinal resistance showed a sharp dip at low magnetic field, *B*, demonstration the WAL behavior, as shown in Figure 4 (bottom). The WAL phenomenon demonstrates both the Dirac nature of the surface state carriers as well as the strong spin−orbit interaction in pristine TI materials[32]. On doping the Sb_2Te_3 film with Cr, the WAL response disappears and instead, an increase in the resistance at low fields corresponding to the MR effect is observed (Figure 4, top). We further obtained the trend comparing the anomalous Hall conductivity, ${\sigma_{xy}}^A$, as a function of temperature for the $Cr_{0.15}Sb_{1.85}Te_3$ samples as shown in Figure 4(b). The curve shows a concave trend over a broad temperature range, similar to the transport data reported by Chang et al.[27], but different from that of Zhou et al.[33] in their SQUID data (both in Cr-doped TIs). Theoretically, T_c can be established as the point when ${\sigma_{xy}}^A$ and H_c both fall to zero at zero magnetic field, but in experiments, a tail is commonly observed above T_c. This may be due to sample inhomogeneity or a finite remnant field arising from the superconducting magnetic coils in the cryostat[34]. Furthermore, the transport measurement is more bulk type measurements which probes the entire thickness of the film, which might account for the slight discrepancy with THz measurements[35]. In order to further our understanding and elucidate the mechanism of magnetism, a detailed study was carried out to comprehend the relationship between carrier densities, *Tc*, and Cr concentration trends using terahertz time domain spectroscopy (THz-TDS), which is discussed in the next section.

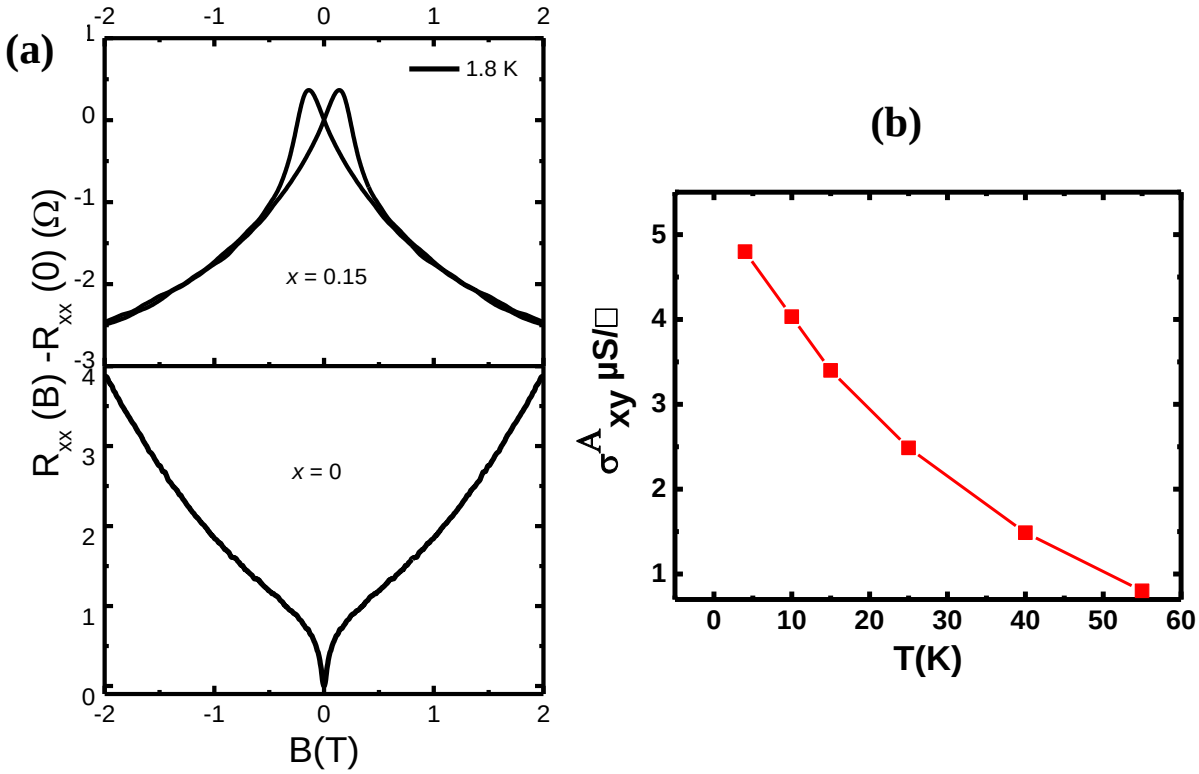

Figure 4. (a) Normalized longitudinal resistance of an undoped Sb_2Te_3 showing the WAL effect compared to a $Cr_xSb_{2-x}Te_3$ sample with x = 0.15. (b) Zero-field anomalous Hall conductivity ($\sigma_{xy}{}^{A}$) for samples with x = 0.15 as a function of temperature.

3. TERAHERTZ RESPONSE BY VARYING Cr DOPING IN $Cr_XSb_{2-X}Te_3$

It is well-known that device processing makes it more challenging to probe the surface states of pristine TI thin films[36], as TI surface states are very sensitive to water and organic solvents. To circumvent this issue, we employed contact-free and non-invasive THz–TDS to determine the carrier densities and mobilities for all the samples. The carrier damping rate in TIs (typically~10^{-13} s^{-1}) lies in the THz frequency range (0.1-2.0 THz), making broadband THz spectroscopy a particularly sensitive probe of TI carrier dynamics. Moreover, the energies typical of collective quasiparticles such as optical phonons, have a fingerprint across the energetic range of the THz radiation (0.4 - 4 meV) making it a powerful technique to study TIs.[32,37,44] The time-resolved THz transmission through $Cr_xSb_{2-x}Te_3$ thin films with varying Cr concentration (x = 0.15,0.41, 0.58, 0.76) was measured at 4 K as shown in Figure 5(a). The primary transmitted THz field intensity shows a systematic reduction with increasing Cr concentration x [Figure 5(a)] which signifies an increased free carrier absorption in the film. To further quantify this behaviour, we extracted the carrier densities and mobilities for each sample as a function of Cr concentration and T_C.

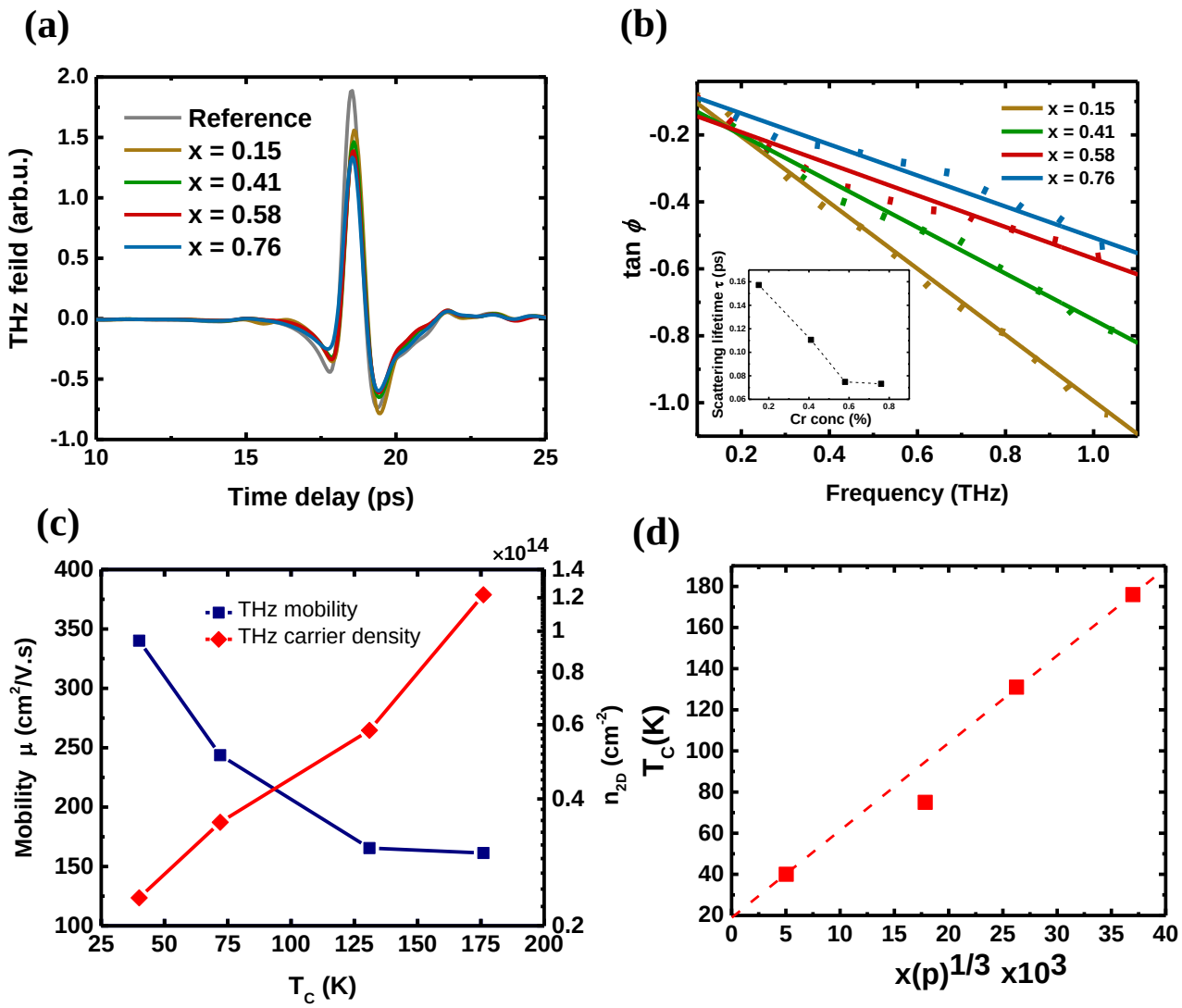

Figure 5. (a) Time domain picosecond pulse response transmitted through 20 QL $Cr_xSb_{2-x}Te_3$ films with varying Cr concentrations *x*. (b) Plot of $\tan\phi$ vs frequency. The solid lines represent the linear fit to each data set. The inset shows the scattering lifetime τ vs Cr concentrations *x*. (c) The plots of mobility μ and carrier density *p* vs Curie temperature *Tc* deduced from the THz measurements (blue and red curves). (d) Sheet carrier density, $p^{1/3}$ *x*, as a function of T_c obtained from the THz measurements.

Using the Tinkham's equation for thin films[38] and substituting for the complex Drude conductivity as $\tilde{\sigma}(\omega) = \sigma_0/(1 - i\omega\tau)$, we obtain the following relationship between the imaginary and the real parts of the transmission coefficient: $Im.\{\tilde{T}(\omega)\}/Re.\{\tilde{T}(\omega)\} = -\omega\tau = \tan\phi$, where ϕ is the phase angle between the sample and substrate waveforms, ω is the angular frequency and τ is the scattering lifetime for the carriers. Plotting $\tan\phi$ as a function of frequency [Figure 5(b)], and fitting it with a linear regression, the slope yields the scattering lifetime τ [inset to Figure 5(b)]. Furthermore, the scattering lifetime τ, obtained from THz-TDS, was used to calculate the THz mobility using $\mu = \tau e/m^*$(assuming the bulk hole effective mass m^* in Sb_2Te_3 is 0.78 m_e, with m_e as the electron rest mass), as shown in Figure 5(c).The carrier concentration p can then be obtained using the following relationship between sheet conductance G_{2D} and p: $G_{2D} = G(\omega \to 0) = \mu ep$. This yields the plot shown in Figure 5(c), and in principle can be directly compared the values of p and μ extrapolated from the slope of R_{xy} vs B at high fields. The carrier densities (and mobilities) in the THz measurements increase (decrease) roughly linearly with the Curie temperature T_c (T_c for x = 0.41, 0.58, 0.76 is obtained from Ref. 39] yielding the carrier dependence of the magnetic ordering temperature. It is interesting to note that the values of p obtained from the THz measurements tend to be smaller than those deduced from the Hall transport measurements. We used the

bulk hole effective mass $m^* = 0.78\ m_e$ in calculating the values for the THz measurements[39]. Due to the anisotropic nature of the upper and lower valence bands in Sb_2Te_3 the effective mass varies from $m^* = 0.034\ m_e$ to $m^* = 1.24\ m_e$[40,41]. This is likely to be one of the origins for the quantitative discrepancy in the parameters obtained from THz and transport measurements. Furthermore, Ar^+ ion milling used during the Hall bar processing has been reported to increase the transport carrier density in topological insulators[42]. Figure 5(d) shows the relationship between T_c and $xp^{1/3}$. In the scenario when magnetism between two localised spin is mediated through carriers in the mean field approximation, the Curie temperature is given by[43]: $T_c = \frac{S(S+1)}{3k_B} nJ^2\chi$, where S is the spin quantum number of Cr, n is the number density of Cr in the material, J is the exchange interaction constant between localized Cr spin and itinerant holes, and χ is susceptibility of itinerant hole spins. In the above equation, χ can be further described in terms of Fermi wave vector (k_F) as: $= \frac{m^*}{h^2} k_F = \frac{m^*}{h^2}(3\pi^2 p)^{\frac{1}{3}}$, where m^* is hole effective mass, h is Planck constant, and p is hole density. Together the two equations indicate that in mean field theory, T_c will be proportional to $xp^{1/3}$. We plotted T_c with respect to $xp^{1/3}$ in all samples with results obtained from electrical transport and THz measurements [Figure 5(d)]. Our results demonstrate a good proportionality between T_c and $xp^{1/3}$, clearly supporting the validity of the mean field approximation in the parabolic band model, and strongly suggesting RKKY mediated magnetism in our $Cr_xSb_{2-x}Te_3$ films. This behaviour is similar to that reported by Zhou et al.[33] and Li et al[45]. In addition, this illustrates the proportionality between the Cr concentration x and the carrier density p with a monotonic increase in p with x also consistent with the mean field theory.

4. CONCLUSION

In conclusion, we used THz spectroscopy and magneto-transport to carry out a detailed study of ferromagnetism in in 20-nm-thick magnetically doped $Cr_xSb_{2-x}Te_3$ TI thin films. The temperature dependent behavior of the THz conductance revealed a metallic behavior below 40 K, indicating that the ferromagnetic order in the $Cr_xSb_{2-x}Te_3$ is via the carrier-mediated RKKY mechanism. Magneto-transport measurement showed an anomalous Hall effect behaviour as a function of magnetic field and temperature, confirming out-of-plane ferromagnetic ordering in $Cr_xSb_{2-x}Te_3$. We measured a T_c of ~40 K for the lowest doped sample from the THz measurements, consistent with the T_c value obtained from the transport measurements. On plotting carrier densities and mobilities for all Cr doped samples obtained entirely from optical THz-TDS, we found that the T_c value was proportional to $xp^{1/3}$. This directly suggests a strong correlation between carrier concentration and ferromagnetism originating from a mean field approximated RKKY interaction scenario. Our work presents a unique comparison of optical measurements using THz-TDS and electrical transport measurements to achieve a complete characterization of Cr doping in Sb_2Te_3 thin films and their ferromagnetic properties. Moreover, these results provide a new pathway to explore quantum phenomena based on the magnetically induced gap opening at the Dirac point in topological insulators.

5. ACKNOWLEDGMENTS

The authors of this manuscript acknowledge financial support from the Engineering and Physical Sciences Research Council (EPSRC), grant numbers KLZA/145 – High precision terahertz spectroscopy and microscopy (HyperTerahertz) and the Cambridge Commonwealth Trust.

REFERENCES

(1) Klitzing, K.; Dorda, G.; & Pepper. M.; New Method for High-Accuracy Determination of the Fine Structure Constant Based on Quantized Hall Resistance. *Phys. Rev. Lett*. **45**, 494 (1980).
(2) Moore, J. E. & Balents, L. Topological invariants of time-reversal-invariant band structures. *Phys. Rev. B* **75,** 121306 (2007).
(3) Fu, L., Kane, C. L. & Mele, E. J. Topological Insulators in Three Dimensions. *Phys. Rev. Lett.* **98,** 106803 (2007).
(4) Hasan, M. Z. & Kane, C. L. Colloquium: Topological insulators. *Rev. Mod. Phys.* **2011,** 3045–3067 (2011).
(5) Moore, J. E. The birth of topological insulators. *Nature* **464,** 194–198 (2010).
(6) Liu, Q., Liu, C. X., Xu, C., Qi, X. L. & Zhang, S. C. Magnetic impurities on the surface of a topological insulator. *Phys. Rev. Lett.* **102,** 156603, 1–4 (2009).

(7) Chen, Y. L. *et al.* Massive Dirac Fermion on the Surface of a Magnetically Doped Topological Insulator. *Science* **329,** 659–662 (2010).
(8) Dziom, V. *et al.* Observation of the universal magnetoelectric effect in a 3D topological insulator. *Nat. Commun.* **8,** 15197 (2017).
(9) Qi, X.-L., Li, R., Zang, J. & Zhang, S.-C. Inducing a Magnetic Monopole with Topological Surface States. *Science* **323,** 1184–1187 (2009).
(10) Yu, R. *et al.* Quantized Anomalous Hall Effect in Magnetic Topological Insulators. *Science* **329,** 61–64 (2010).
(11) Fujita, T., Jalil, M. B. A. & Tan, S. G. Topological insulator cell for memory and magnetic sensor applications. *Appl. Phys. Express* **4,** 094201 (2011).
(12) Wang, Q. *et al.* Characterization of Cr-doped Sb_2Te_3 films and their applications to phase-change memory. *Phys. status solidi - Rapid Res. Lett.* **9,** 470–474 (2015).
(13) Huang, Y. Q., Song, Y. X., Wang, S. M., Buyanova, I. A. & Chen, W. M. Spin injection and helicity control of surface spin photocurrent in a three dimensional topological insulator. *Nat. Commun.* **8,** 15401 (2017).
(14) Collins-McIntyre, L. J. *et al.* Structural , electronic , and magnetic investigation of magnetic ordering in MBE-grown $Cr_xSb_{2-x}Te_3$ thin films. *EPL (Europhysics Letters)* **115,** 27006 (2016).
(15) Nagaosa, N., Sinova, J., Onoda, S., MacDonald, A. H. & Ong, N. P. Anomalous Hall effect. *Rev. Mod. Phys.* **82,** 1539–1592 (2010).
(16) Chang, C.-Z. *et al.* High-precision realization of robust quantum anomalous Hall state in a hard ferromagnetic topological insulator. *Nat. Mater.* **14,** 473 (2015).
(17) Chang, C.-Z. *et al.* Experimental Observation of the Quantum Anomalous Hall Effect in a Magnetic Topological Insulator. *Science* **340,** 167–170 (2013).
(18) Li, M. *et al.* Experimental Verification of the Van Vleck Nature of Long-Range Ferromagnetic Order in the Vanadium-Doped Three-Dimensional Topological Insulator Sb_2Te_3. *Phys. Rev. Lett.* **114,** 146802 (2015).
(19) Duffy, L. B. *et al.* Magnetic proximity coupling to Cr-doped Sb_2Te_3 thin films. *Phys. Rev. B* **95,** 224422 (2017).
(20) Das, D. *et al.* Defect induced structural and thermoelectric properties of Sb_2Te_3 alloy. *J. Appl. Phys.* **118,** 045102 (2015).
(21) Nuss, M. C. & Orenstein, J.; *Millimeter and Submillimeter Wave Spectroscopy of Solids*. Springer-Verlag Berlin Heidelberg, 1998; pp 7-50.
(22) Park, S. H. *et al.* Reversible Fermi Level Tuning of a Sb_2Te_3 Topological Insulator by Structural Deformation. *Nano Lett.* **15,** 3820–3826 (2015).
(23) Park, B. C. *et al.* Terahertz single conductance quantum and topological phase transitions in topological insulator Bi_2Se_3 ultrathin films. *Nat. Commun.* **6,** 6552 (2015).
(24) Von Molnar, S. & Kasuya, T. Evidence of band conduction and critical scattering in dilute Eu-chalcogenide alloys. *Phys. Rev. Lett.* **21,** 1757–1761 (1968).
(25) Kasuya, T. A Theory of Metallic Ferro- and Antiferromagnetism on Zener's Model. *Prog. Theor. Phys.* **16,** 45–57 (1956).
(26) Ye, M. *et al.* Carrier-mediated ferromagnetism in the magnetic topological insulator Cr-doped $(Sb,Bi)_2Te_3$. *Nat. Commun.* **6,** 8913 (2015).
(27) Chang, C. *et al.* Field-effect modulation of anomalous Hall effect in diluted ferromagnetic topological insulator epitaxial films. *Sci. China Physics, Mech. Astron.* **59,** 637501 (2016).
(28) Žutić, I., Fabian, J. & Sarma, S. Das. Spintronics: Fundamentals and applications. *Rev. Mod. Phys.* **76,** 323–410 (2004).
(29) Fert, A. Nobel Lecture: Origin, development, and future of spintronics. *Rev. Mod. Phys.* **80,** 1517–1530 (2008).
(30) Nguyen, T. *et al.* Topological states and phase transitions in Sb_2Te_3-GeTe multilayers. *Sci. Rep.* **6,** 27716 (2016).
(31) Lang, M. *et al.* Competing Weak Localization and Weak Antilocalization in Ultrathin Topological Insulators. *Nano Lett.* **13,** 48–53 (2013).
(32) Kamboj, V. S.; Singh, A.; Ferrus, T.; Beere, H. E.; Duffy, L. B.; Hesjedal, T.; Barnes, C. H. W. & Ritchie, D. A. Probing the Topological Surface State in Bi_2Se_3 Thin Films Using Temperature-Dependent Terahertz Spectroscopy. *ACS Photonics* **4**, 2711-2718 (2017).
(33) Zhou, Z., Chien, Y. & Uher, C. Thin film dilute ferromagnetic semiconductors $Sb_{2-x}Cr_xTe_3$ with a Curie temperature up to 190 K. *Phys. Rev. B* **74,** 224418 (2006).
(34) Wang, M. *et al.* Three-dimensional Heisenberg critical behavior in the highly disordered dilute ferromagnetic semiconductor (Ga,Mn)As. *Phys. Rev. B* **93,** 184417 (2016).

(35) McCord, J. Progress in magnetic domain observation by advanced magneto-optical microscopy. *J. Phys. D. Appl. Phys.* **48,** 333001 (2015).
(36) Benia, H. M.; Lin, C.; Kern, K. & Ast, C. R. Reactive Chemical Doping of the Bi_2Se_3 Topological Insulator. *Phys. Rev. Lett.* **107**, 177602, (2011).
(37) Kamboj, V.S.; Singh, A.; Ferrus, T.; Beere, H.; Duffy, L.; Hesjedal, T.; Barnes, C.; Ritchie, D. Temperature evolution of topological surface states in Bi_2Se_3 thin films studied using terahertz spectroscopy. *Proc. of SPIE*, **10103**, 101030D-1 (2017).
(38) Grüner, G. *Millimeter and submillimeter wave spectroscopy of solids*. *Topics in Applied Physics.* Springer **74** (1998). doi:10.1007/BFb0103417.
(39) Singh. A., Kamboj, V.S., Liu, J., Llandro, J., Duffy, L.B., Senanayak, S.P., Beere, H.E., Ionescu, A, Ritchie, D.A., Hesjedal, T., &Barnes, C.H.W. Systematic Study of Ferromagnetism in $Cr_xSb_{2-x}Te_3$ Topological Insulator Thin Films using Electrical and Optical Techniques, *Sci. Rep.* **8**, *17024*, (2018).
(40) O. Madelung, Semiconductors: Data Handbook, 3rd ed.Springer, Berlin (2004)
(41) Takagaki, Y., Giussani, A., Perumal, K., Calarco, R. & Friedland, K. J. Robust topological surface states in Sb_2Te_3 layers as seen from the weak antilocalization effect. *Phys. Rev. B* **86,** 125137 (2012).
(42) Banerjee, K. *et al.* Defect-induced negative magnetoresistance and surface state robustness in the topological insulator $BiSbTeSe_2$. *Phys. Rev. B* **90,** 235427 (2014).
(43) Jungwirth, T. *et al.* Prospects for high temperature ferromagnetism in (Ga,Mn)As semiconductors. *Phys. Rev. B* **72,** 165204 (2005).
(44) Kamboj, V. S.; Singh, A.; Ferrus, T.; Beere, H. E.; Duffy, L. B.; Hesjedal, T.; Barnes, C. H. W. & Ritchie, D. A. THz carrier dynamics and magnetotransport study of topological surface states in thin film Bi_2Se_3. *Proc. SPIE. 10531, Terahertz, RF, Millimeter, and Submillimeter-Wave Technology and Applications XI;* ***105310I***, (2018).
(45) Li, B. *et al.* Carrier dependent ferromagnetism in chromium doped topological insulator $Cr_y(Bi_xSb_{1-x})_{2-y}Te_3$. *Phys. Lett. A* **377,** 1925–1929 (2013).